18TH WORLD CONFERENCE ON EARTHQUAKE ENGINEERING
WCEE2024
MILAN

MILAN, ITALY
30TH JUNE - 5TH JULY 2024

www.wcee2024.it

THE 2019 E-DEFENSE SHAKE-TABLE TEST OF A LARGE-SCALE 3-STORY DISASTER MANAGEMENT CENTER

K. Kusunoki[1], TZ. Yeow[1], T. Seike[2], S. Yagi[2], A. Teramoto[3], I. Nakamura[4], Y. Hibino[5], & S. Fukai[6]

[1] Earthquake Research Institute, University of Tokyo

[2] Building Research Institute, Tsukuba

[3] Graduate School of Advanced Science and Engineering, Hiroshima University

[4] Department of Nuclear Safety Engineering, Tokyo City University

[5] Graduate School of Environmental Studies, Nagoya University

[6] Design Technology Center, Nikken Sekkei

Abstract: In December 2019, shake-table tests of a 3-story disaster management center were performed at E-Defense in Japan as part of the Tokyo Metropolitan Resilience Project. This large-scale test was a collaboration between universities and research institutes in Japan and the US NHERI Natural Hazards Reconnaissance (RAPID) facility. Research objectives include validating resilient structural and non-structural element detailing and verifying the accuracy of a newly proposed structural health monitoring technique.

The specimen was a reinforced concrete frame building, with spandrel walls cast to be monolithic with frame elements to provide additional strength and stiffness. Special detailing was provided to prevent early wall damage caused by bar buckling. The building remained mostly elastic during an excitation equivalent to a severe earthquake motion defined in the Japanese Building Standard Law and survived multiple 50%-60% more severe events without collapsing. This demonstrates that the spandrel wall detailing was a good solution for buildings requiring post-disaster functionality.

Other non-structural elements, such as ceilings, windows, and wall tiles, were installed. Two variants of each were constructed, one using typical Japanese detailing and another using more resilient detailing (e.g., flexible adhesive for wall tiles). In all cases, the more resilient variant performed better, demonstrating the effectiveness of the low-damage detailing.

Various structural health monitoring (SHM) methods were applied, such as an inexpensive acceleration sensor network and 3D scanning technology. A new technique was applied to extract the building's capacity curve from recorded acceleration response to classified damage. The results agreed well with resource tensive visual inspections demonstrating the benefits of adopting the new SHM technique in reducing resources required for post-earthquake damage evaluations.

Overall, the shake-table test provided a great opportunity to observe the behavior of a whole building system and provided means to cover a wide range of research disciplines effectively. However, methods to consider soil-structure-interaction effects should be developed for future tests to ensure more realistic building simulations.

1. Introduction

In this research project, as part of this sub-project (c), "2: Immediate safety evaluation and immediate determination of continued usability of disaster base buildings", research and development were conducted, which aimed at building a system that will install sensors to quickly determine the safety of a building, its collapse margin, and whether or not it can be continued to be used after an earthquake. Specifically, a shaking table test was conducted with a real building in which not only the structural frame but also equipment and non-structural members were reproduced through a large-scale shaking table facility. Based on the building response data measured by sensors, a new technique was proposed that can instantly evaluate the level of damage to components and a method for determining the continued usability of facilities based on quantitative evaluation of the margin of collapse.

This research project targets buildings that comply with the Ministry of Land, Infrastructure, Transport and Tourism's “Seismic Design Guidelines for Disaster Management Centre” (hereinafter referred to as Disaster Management Centre)(MILT, 2018). In the guidelines, standing walls, wing walls, and hanging walls are considered as structural elements. However, it is known that flexural reinforcement placed at the end of a wall yields prematurely and then increases damage to the member, as shown in Figure 1 (a). To avoid the damage, the structural gap at the wall end to isolate the wall is recently applied, as shown in Figure 1 (b). However, this detail cannot count as any contribution to the wall. Therefore, a new detail is proposed, in which the compression force is sustained by concrete only on the compression side without anchoring flexural reinforcing bars at the ends, as shown in Figure 1 (c).

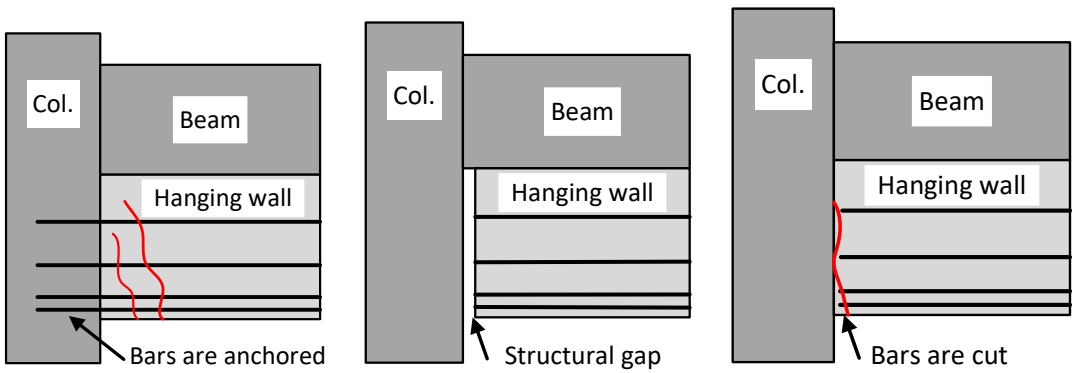

(a) Conventional (b) W/ Structural gap (c) New proposal

Figure 1. Details to anchor the flexural reinforcements.

One of the objectives of the project is to confirm the validity of the system to evaluate the degree of damage to structures using sensors based on safety against aftershocks, using a method that utilizes the equivalent linearization method. Furthermore, its effectiveness will be confirmed through shaking table experiments on a full-scale three-story reinforced concrete building (Trevor TZ. Et.al. 2020).

2. Outline of the shaking table test

2.1. Outline of the test specimen

The specimen was shaken in one direction. The test specimen had two spans in the vibration direction and one span in the perpendicular direction. Figure 2 shows the dimensions of the test specimen. The building height is 10.7m. In the excitation direction, wing walls, standing walls, and hanging walls are arranged. A structural gap with a width of 5 cm is provided between the standing wall/hanging wall of the 2nd and 3rd-floor

beams and the wing wall. Additionally, there is a 0 cm wide slit (in other words, the horizontal reinforcement in the hanging wall is not anchored) between the hanging wall and the wing wall on the R floor. The test specimen was designed to satisfy Category I of the “Functional Continuity Guidelines for Buildings Serving as Disaster Prevention Bases" issued by the Ministry of Land, Infrastructure, Transport and Tourism in 2018. The required performance for Class I is a maximum inter-story deformation angle of 1/300 or less, a base shear coefficient of 0.55 or more, and a member yielding factor of 1.0 or less, and according to the guidelines, it can maintain functionality up to an input of approximately 1.5 times the required seismic motion level.

The exterior wall tiles were installed between ① and ② on one structural surface in the excitation direction and were glued with elastic adhesive from the center between ① and ② toward the outer columns and with mortar between the middle columns. Additionally, the ceiling was installed between ② and ③ on the 2nd and 3rd floors, with the 2nd floor being designed as a non-earthquake-resistant ceiling and the 3rd floor as an earthquake-resistant ceiling.

In the experiment, accelerometers, laser transducers, and optical sensors were placed on each floor to measure response acceleration and inter-story deformation. The locations of the sensors are also shown in Figure 2 (b).

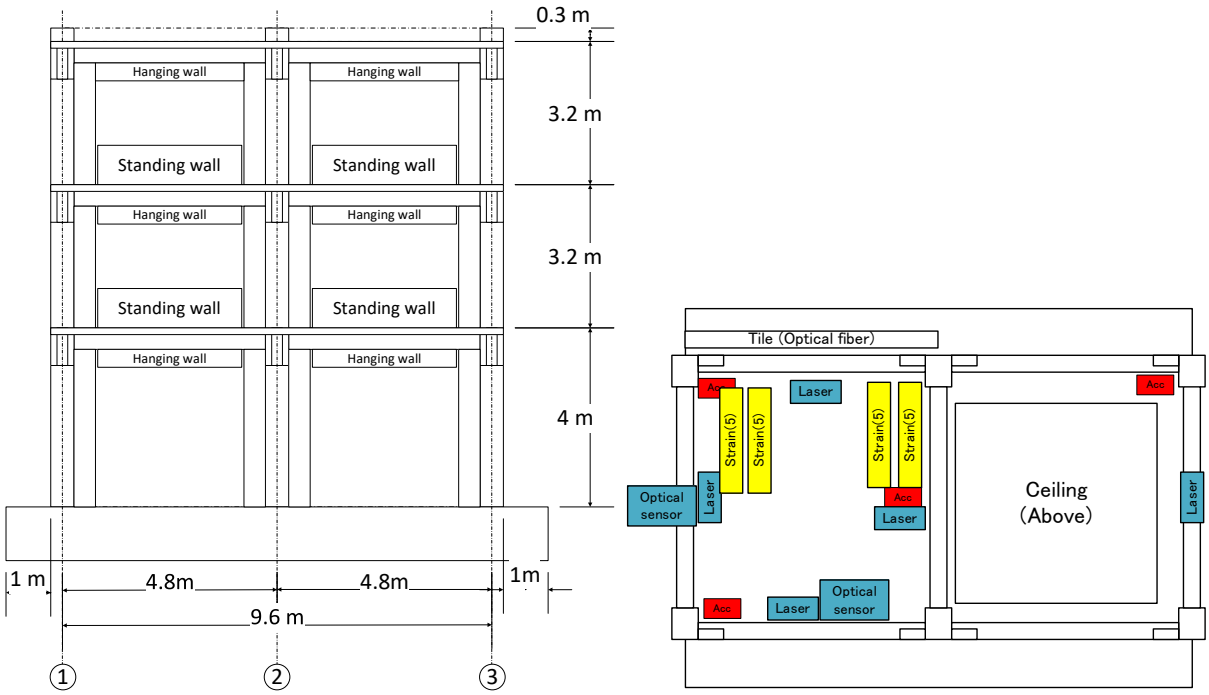

(a) Elevation (b) Plan

Figure 2. Dimensions of the test specimen.

A steel column was erected from the beams on the upper and lower floors to install the laser transducers, and the distance between the two columns was measured using a laser displacement meter. In addition, in order to measure the deflection angle of the column, two laser transducers were placed at different height positions in the center of the floor.

In this study, two types of acceleration sensors were used: a high-precision MEMS type (LAM02) and an inexpensive one for educational use (ADXL355). There is a difference of about 20 times in price, and the performance of each is shown in Table 1.

Table 1. Accelerometers.

	LAM02	ADXL355
Period (kHz)	1.7	2.4
Sensitivity (mV/G)	400	400
Range (G)	±2.5	±2.0
Resolution (bit)	24	20
Minimum acceleration($\times 10^{-3}$cm/s^2)	0.15	1.87
Nonlinearity	Less than 0.3%	0.1%

2.1. Input motion

An artificial seismic wave was used as the input seismic wave. The design target spectrum at the engineering bedrock defined in the notification by the ministry was applied for the target spectrum. The spectrum was then amplified with the soil layer amplification factor of Gs for the ordinary soil condition (Type 2). For the phase spectrum, the NS component of the JMA Kobe wave was applied. Since the test specimen is 80% of the actual size, the time axis was multiplied by $\sqrt{}0.80$.

The excitation was carried out over three days, as shown in Table 2. On the first day, 20% of the artificial seismic wave input and 100% of the design level for general buildings were input to confirm continuous usability. On the second day, we entered the design target of 150% for this building. On the third day, assuming the maximum aftershock, 150% was input again, and finally, 160% was applied, which was the excitation limit of the shaking table. Before and after each seismic motion input, white noise waves were input in three directions separately in order to measure the dynamic characteristics of the test specimen. Since it is not possible to observe damage to the test specimen unless the oil pressure is lowered immediately, the state of damage to the test specimen was confirmed at the end of each shaking day.

Table 2. Input motions.

Day 1	No	Input
	1	White noise
	2	20% (Damage limit state)
	3	White noise
	4	100% (Safety limit state)
	5	White noise
Day 2	6	White noise
	7	150% (For disaster management center)
	8	White noise
Day 3	9	White noise
	10	150% (Aftershock)
	11	White noise
	12	160% (Upper limit of the table)
	13	White noise

3. Test results

3.1. Outline of the test results

Table 3 shows the maximum response acceleration and maximum inter-story deformation angle of each story for each input. The maximum response acceleration was measured by LAM02 installed at the center of the test piece, and the maximum inter-story deformation angle was measured with the laser displacement meter at the center of the floor. At 20% input, the maximum inter-story deformation angle for each layer was sufficiently small, and it appears to be within the elastic range. Even at 100% input, the maximum interlayer deformation angle was 1/292 (one layer), and although cracks did occur, it is thought to be near the second bending point on the performance curve. The deformation progressed significantly from 150% input, reaching

1/65 (1st story) with the first 150% input, and further deformed with the second input, reaching 1/43 (1st story). In the end, I reached about 1/30th with 160% input.

Table 3. Maximum responses.

Run	1F		2F		3F	
	Peak Acc. (cm/sec^2)	Max. Drift angle	Peak Acc. (cm/sec^2)	Max. Drift angle	Peak Acc. (cm/sec^2)	Max. Drift angle
20%	140	1/3828	190	1/3800	221	1/5970
100%	690	1/292	944	1/330	1085	1/873
150%	1103	1/65	1340	1/71	1714	1/128
150%	1245	1/43	1434	1/45	1619	1/92
160%	1079	1/29	1382	1/30	1590	1/59

3.2. Structural health monitoring with accelerometers

Figure 3 shows the performance curve measured at the second 150% input, the tri-linear model estimated at the first 150% input, the predicted maximum response point for the maximum aftershock, the maximum response point at the first 150% input, and the evaluated damage classes according to the method proposed by Pan and Kusunoki (2020). In the first 150% input, both the positive and negative sides were determined to be severely damaged (IV), and from the response point to the predicted maximum displacement during the aftershock, it was estimated that the building would collapse (V) due to the aftershock. In fact, on the second 150% input, the maximum response displacement on the negative side exceeded the limit point that the building could withstand (called the safe limit point) and reached the level of collapse, indicating that the judgment was on the safe side.

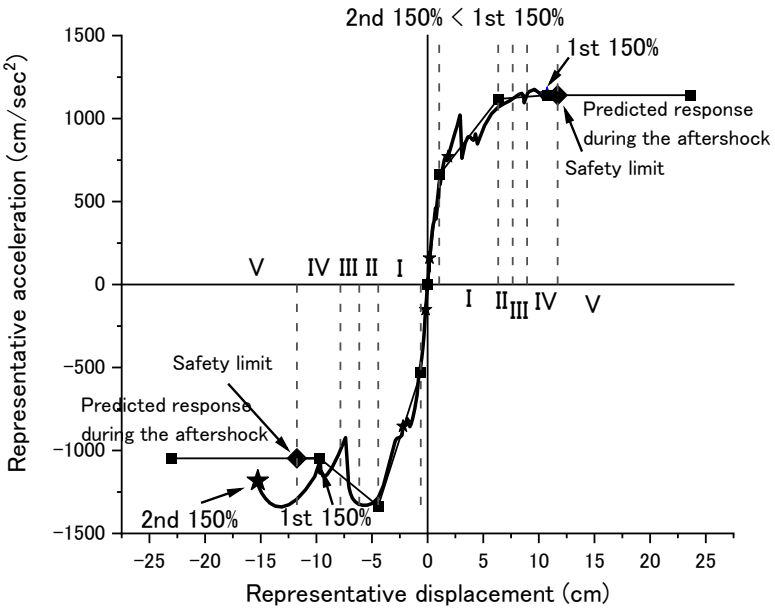

Figure 3. Response prediction point at the first 150% input and response at the second 150% input.

3.3. Finishing tiles

Spalling of exterior tiles occurs not only during earthquakes but also due to subsequent aftershocks and environmental changes. Therefore, in order to determine whether to continue using the building after an earthquake, it is important to detect the spalling state of the exterior tiles.

It is thought that the peeling of exterior tiles can be evaluated by the strain difference between the tile and the underlying concrete. Therefore, by using an ultra-thin diameter optical fiber sensor, peeling detection

monitoring was carried out in an environment that does not affect the adhesion performance of the tiles. Tiles were installed using two different adhesives: mortar and elastic adhesive.

As a result of the shaking table test, it was found that the deterioration of the tiles was concentrated around the bottoms of the column and structural gaps where structural cracks tend to occur, and that in addition to spalling, cracks that penetrated the tiles occurred in the areas with mortar adhesive. It was found that there were no spalling or cracks in the elastic adhesive-covered area, but a large number of peelings occurred. An example of tile deterioration is shown in Figure 4.

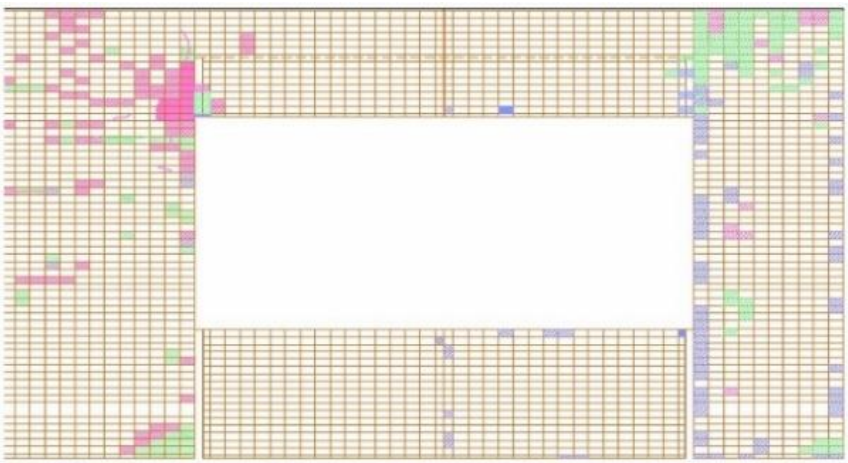

Figure 4. Tile deterioration status after final vibration of each day. Blue: Dec. 3, Green: Dec. 4, Red: Dec. 6,

The hatch, fill, and solid line indicate the location of peeling, spalling, and crack, respectively.

In addition, an optical fiber sensor near the peeled tile observed a significant strain difference between the tile and the underlying concrete and a phenomenon in which the followability of the tile decreased before and after peeling was confirmed, as shown in Figure 5. it was confirmed that it is possible to instantly determine the risk of peeling of exterior tiles by using optical fiber sensors.

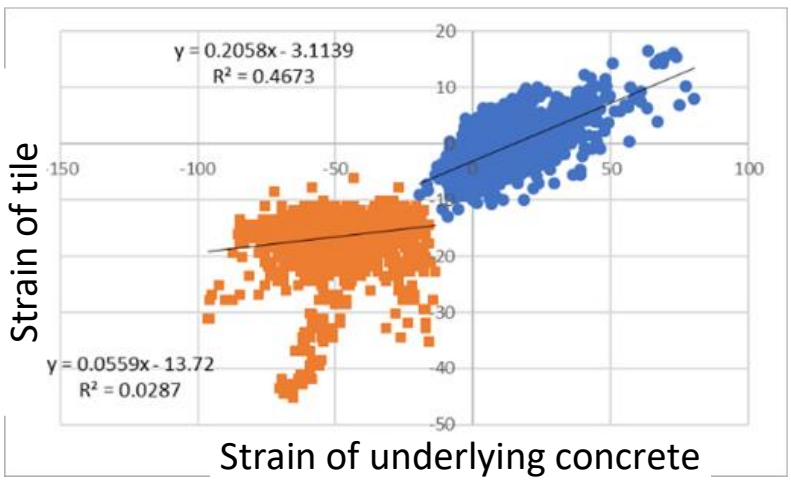

Figure 5. Stains of tile and underlying concrete.

3.4. Window frame

Fixed double-sided windows and sliding windows were installed on the second and third floors. On the third floor, a large window with a size of 1,650 x 1,440 mm and a total thickness of 8 mm was installed. Two 790 x 1,440 mm inset windows were installed on the second floor, where the angle of inter-story deformation was expected to be larger than on the third floor. Additionally, sliding windows of 1,490 x 1,440 mm with a thickness of 4 mm were installed on each floor (Figure 6).

(a) 2nd floor (b) 3rd floor

Figure 6. Stains of tile and underlying concrete.

At 100% input, the horizontal displacement of the glass relative to the sash of the fixed window was a maximum of 4 mm on the second floor and approximately 2.5 mm on the third floor. At 150% input, the deformation of the second floor exceeded the tolerance of the measuring transducer, and the exact value is unknown. However, the maximum displacement in the negative direction was about 15 mm. Furthermore, the displacement on the third floor reached a maximum of about 10 mm. In the case of a fixed window, at 100% input, the maximum value was 8 mm on the second-floor column side, about 5 mm on the center side, about 7 mm on the third-floor column side, and about 3 mm on the center side. At 150% input, the displacement on both the second and third floors exceeded the tolerance of the measuring transducers, and the exact value is unknown. However, the displacement in the positive direction reached a maximum of about 10 mm.

After 100% input, slight cracks were confirmed in the mortar filled between the window and the frame, and the crescent of the sliding window was beginning to open. After 150% input, cracks in the mortar progressed, and the sashes of both the sliding and double-sided windows were slightly damaged. However, the way the sash breaks differs on each floor, with the sash on the second floor having damage, such as the central corner breaking, and the sash on the third floor having a gap at the joint between the horizontal and vertical members of the window. The seal on the window was broken. After 160% input, cracks in the mortar progressed and some of the anchors supporting the sash were exposed. Additionally, the sash joints were severely damaged, and the seals were broken in various places. During the second 150% input, the crescent of the sliding window on the second floor was damaged, and when the input was 160%, the crescent of the third-floor sliding window was damaged and fell off (Figure 7 (a)). Furthermore, after the crescent came off, the sliding window was moving freely during the shaking. Additionally, the upper left side of the window on the 2nd floor was broken when facing the indoor side, and the upper left side of the window on the 3rd floor was broken in the same way as the 2nd floor, and cracks also appeared on the diagonal (Figure 7 (b)).

(a) Sliding window on the 3rd floor (160%) (b) Fixed window on the 3rd floor (160%)

Figure 7. Damage to the windows.

3.5. Ceiling system

Ceilings were installed on the second and third floors of the building structure. The ceiling on the second floor is a standard installation method using JIS19 type without braces. The ceiling on the third floor, where the response acceleration is expected to be larger than that on the second floor, is installed using a standard earthquake-resistant ceiling of 40 type, with braces and clearance. A 12mm rock wool decorative sound-absorbing board was attached to the 12.5mm gypsum board on both ceilings (Figure 8 and Figure 9).

In this experiment, in order to measure the response acceleration of the ceiling, acceleration sensors were installed at 5 locations on the ceiling surface of the 2nd floor (center and four corners) and at 7 locations on the ceiling surface of the 3rd floor (in addition to the center and four corners, one each near the brace in the applied direction and its vertical direction). In addition, a total of eight cameras were installed on each floor, two under the ceiling and two behind the ceiling, to record the state of the ceiling when force was applied. In addition, visual damage observation was performed after 100% artificial wave input, after the first 150% input, and after 160% input.

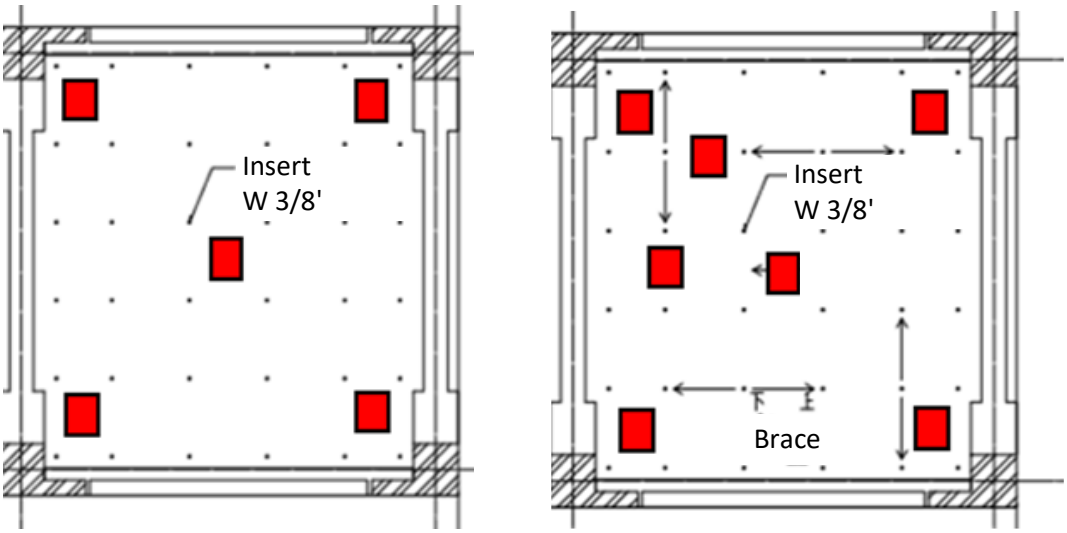

(a) Ceiling for the 2nd floor (b) Ceiling for the 3rd floor

Figure 8. Installed ceiling system.

(a) behind the ceiling (b) ceiling (3rd floor)

(a) behind the ceiling (b) ceiling (3rd floor)

Figure 9. Photos of the ceiling systems.

Figure 10 shows the measurement results of the accelerometer attached to the center of the ceiling at 100% input. Although the floor acceleration is higher on the third floor, the ceiling acceleration is lower on the earthquake-resistant ceiling on the third floor. At 150% input, the peak acceleration of the ceiling on the second floor reached over 60m/sec², so it is thought that the end collided with the beam.

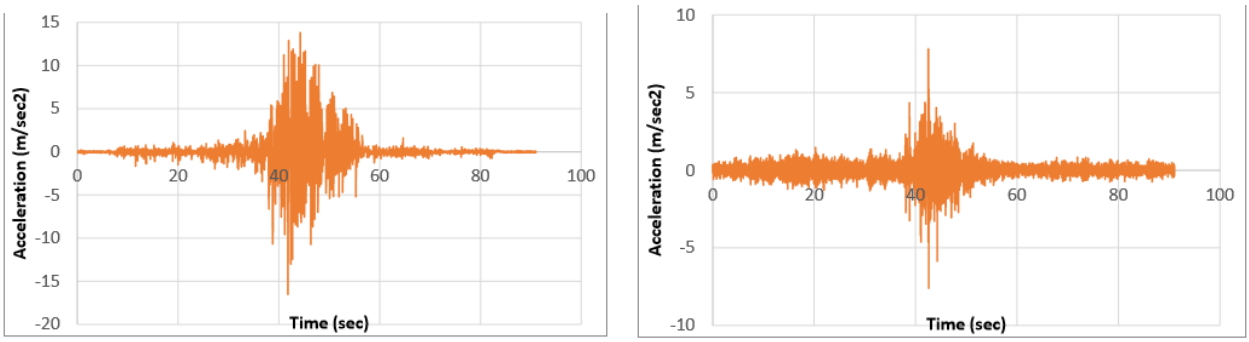

(a) 2nd floor (b) 3rd floor

Figure 10. Accelerations measured at the center of the ceiling (100%).

The visual observation showed no particular damage to the ceilings on the second and third floors after the 100% input. After the first 150% input, it was confirmed that the corners of the ceiling on the second floor were slightly deformed. This is thought to be due to the end colliding with the beam. After 160% input, this deformation occurred on the entire side of the ceiling, and it was confirmed that there was a gap between the beam and the ceiling. Deformation of the board was also confirmed around the inspection port.

3.6. Piping equipment on the roof

Figure 11 shows the measurement plan for foundation piping equipment on the rooftop floor. Figure 12 shows an example of measured displacement and acceleration data of the piping and foundations. In order to understand the behavior of the piping system before and after vibration, 3D scanning of piping equipment was also conducted. The scanned image is shown in Figure 13. The responses of the piping equipment were successfully recorded.

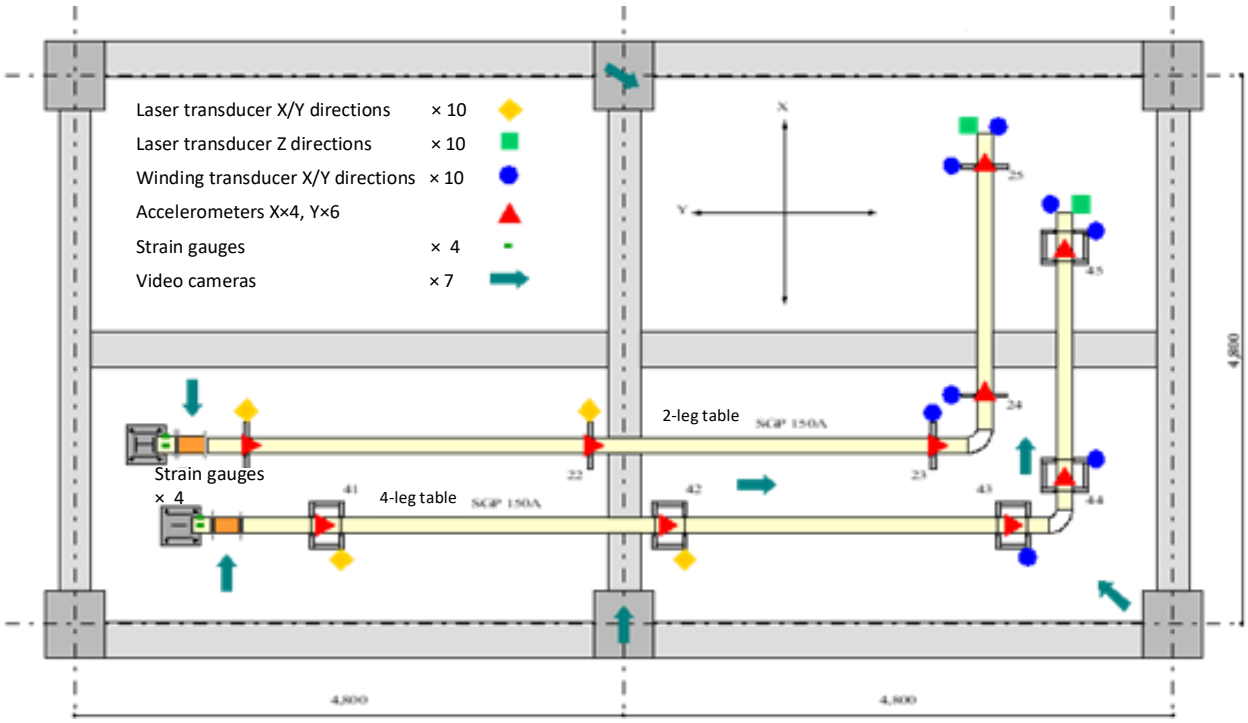

Figure 11. Piping equipment and measurement on the rooftop.

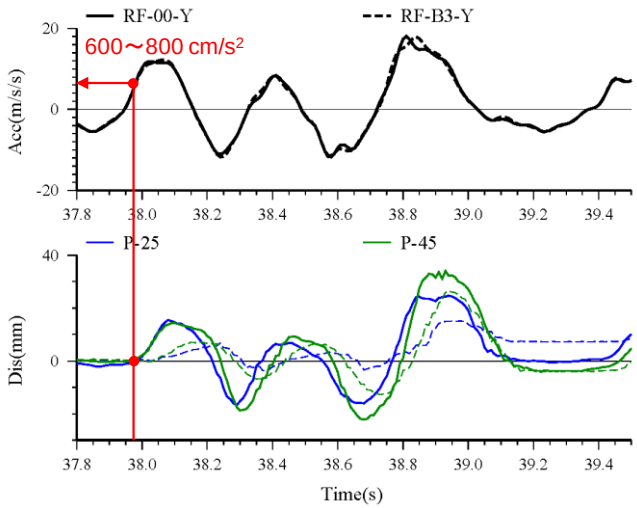

Figure 12. Piping system on the rooftop.

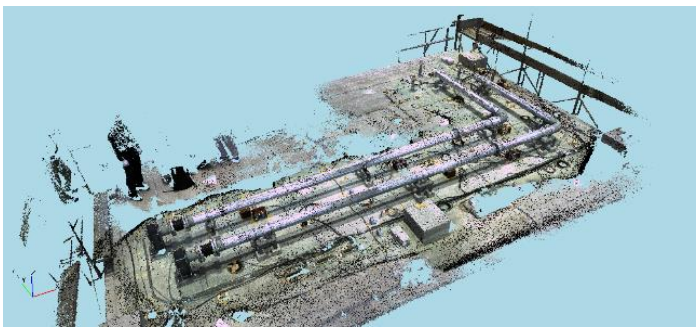

Figure 13. Piping system on the rooftop.

3.7. Damage detection with 3D scanned image

Using a ground-based laser scanner, the following steps were taken to appropriately evaluate damage to the structural specimen (Figure 14).

Step 1: Analysis area extraction

When measuring with this device, it includes not only the point group of the building to be analyzed but also the surrounding objects, so the point group of the building to be analyzed is extracted.

Step 2: Noise processing

The three-dimensional point group measured by a ground-based laser scanner contains a lot of noise from measuring objects other than the target object, so noise removal processing is performed to perform highly accurate damage evaluation.

Step 3: Point group quality deterioration suppression processing

The point group measured by a three-dimensional laser scanner contains an error of several millimeters, and when assessing damage to the walls and floors of buildings, it is necessary to measure many data points at the same location and perform statistical processing on the measured values. , performs processing to reduce the above error.

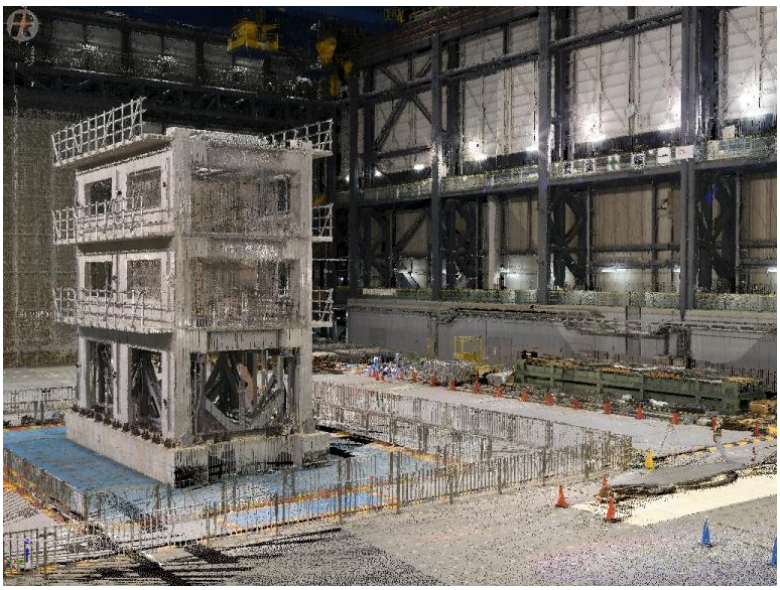

Figure 14. 3D scan image of whole specimen.

After pre-processing the point cloud data according to the items mentioned above, it was investigated whether damage evaluation could be performed by taking the difference between the point group data before and after the shaking. Figure 15 (a) shows the state of the south frame of the test specimen that was damaged after shaking. The exterior walls of the specimen were finished with tiles, and it can be seen that the finish was uneven even before the shaking. For example, the left half of the center column and right beam are shown in blue, indicating that the depth direction's thickness differs due to different construction methods. If the damage to evaluate is a deformation within this construction accuracy, this data is unable to be used for assessing the damage. On the other hand, Figure 15 (b) shows the results obtained by subtracting the data before and after the shaking of the specimen. This figure shows that the colors are almost the same (green) except for the floating tile on the base of the central column on the 1st floor (blue) and the peeling-off tile at the structural gap on the right beam on the 2nd and 3rd floors (red). As such, it is possible to see where the damage occurred. There is a red vertical line in the center of the right beam, which is the location of the red lines at the stepped part between regions where the different adhesives are used to fix the tiles. It can be seen that the width of the red line is getting wider on the upper floors because of the larger residual deformation on the upper floors. Based on the above, it has been shown that the deformation of RC structures can be efficiently evaluated by implementing the series of processes shown here.

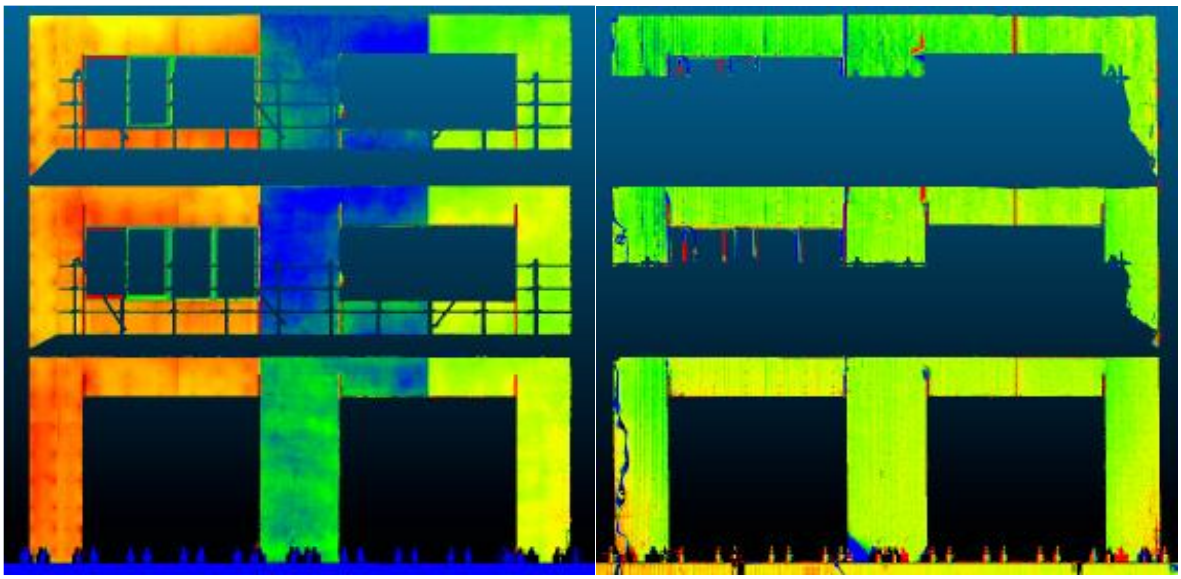

(a) After the shaking (b) Difference before and after the shaking

4. Concluding remarks

A 3-story full-scale reinforced concrete specimen was designed according to the guidelines for the disaster management center. The specimen was shaken on E-Defense to confirm its performance. However, confirming its structural performance is one aspect of assessing the continuous functionality of the building. Damage to the non-structural elements also needs to be assessed. In this test, finishing tiles, window frames, ceiling systems, ceiling systems, and piping equipment are also installed to confirm their damage during strong shaking. Especially for non-structural elements, the scaling effect is not negligible, and the specimen needs to be full-scale. This shaking table test was the first case to collaborate with researchers for structural engineering, material engineering, and non-structural elements. A full-scale shaking table test is costly and takes time to prepare. Researchers of many research fields should be involved in the large-scale shaking table test to utilize the test most efficiently.

5. Acknowledgment

The presented work is supported by the Tokyo Metropolitan Resilience Project of the National Institute for Earth Science and Disaster Resilience. We would also like to acknowledge the many teams and participants involved in the test that enabled it to be a success.

6. References

Hirata N. (2017): Introduction to the Tokyo Metropolitan Resilience Project, NHERI-NIED Plenary Session Presentation

Ministry of Land, Infrastructure, Transport and Tourism(MLIT) (2018): Design guidelines for buildings with post-disaster functions (draft), Technical Note of National Institute for Land and Infrastructure Management, No. 1004

Pan H. and Kusunoki K. (2020): Aftershock damage prediction of reinforced-concrete buildings using capacity spectrum assessments, Soil Dynamics and Earthquake Engineering, Elsevier, 129,105952

Yeow TZ., Kusunoki K., Nakamura I., Hibino Y., Ohkubo T., Seike T., Yagi S., Mukai T., Calvi P., Moustafa M., and Fukai S. (2020): The 2019 Tokyo Metropolitan Resilience Project E-Defense Test of A 3-Story Disaster Management Center, 17th World Conference on Earthquake Engineering